

Inelastic losses in radiofrequency-dressed traps for ultracold atoms

Daniel J. Owens and Jeremy M. Hutson*

*Joint Quantum Centre (JQC) Durham-Newcastle, Department of Chemistry,
Durham University, South Road, Durham DH1 3LE, United Kingdom.*

(Dated: November 21, 2021)

We calculate the rates of inelastic collisions for ultracold alkali-metal atoms in radiofrequency-dressed traps, using coupled-channel scattering calculations on accurate potential energy surfaces. We identify an rf-induced loss mechanism that does not exist in the absence of rf radiation. This mechanism is not suppressed by a centrifugal barrier in the outgoing channel, and can be much faster than spin relaxation, which is centrifugally suppressed. We explore the dependence of the rf-induced loss rate on singlet and triplet scattering lengths, hyperfine splittings and the strength of the rf field. We interpret the results in terms of an adiabatic model of the collision dynamics, and calculate the corresponding nonadiabatic couplings. The loss rate can vary by 10 orders of magnitude as a function of singlet and triplet scattering lengths. ^{87}Rb is a special case, where several factors combine to reduce rf-induced losses; as a result, they are slow compared to spin-relaxation losses. For most other alkali-metal pairs, rf-induced losses are expected to be much faster and may dominate.

I. INTRODUCTION

Radiofrequency-dressed traps [1, 2] have been widely used [3] to confine ultracold atoms in complex geometries, including shells [4] and rings [5]. These geometries are valuable in many fields, including condensate splitting and atom interferometry [6] and the study of low-dimensional quantum systems [7]. The atoms are trapped using a combination of magnetic and radiofrequency (rf) fields, and are confined in an adiabatic potential obtained by diagonalizing a simple Hamiltonian in a basis set of rf-dressed atomic states. Radiofrequency dressing has also been used to form new structures in optical lattices [8, 9].

There are various sources of losses of atoms from rf-dressed traps. The rf-dressed state that is adiabatically trapped is not the lowest that exists, and Burrows *et al.* [10] have considered one-body losses due to nonadiabatic transitions to lower states. Such losses may be made acceptably small by avoiding very low rf coupling strengths. However, the presence of rf radiation introduces additional loss mechanisms that are not present for atoms in a purely magnetic trap, due to rf-induced inelastic collisions.

Tscherbul *et al.* [11] have developed a coupled-channel theory of atomic collisions in rf fields and applied it to rf-induced resonances in ^{87}Rb . Hanna *et al.* [12] developed an approach based on multichannel quantum defect theory, and also explored rf-induced resonances in ^{87}Rb and ^6Li . However, Hanna *et al.* stated that calculations with their method were impractical close to atomic rf transitions, which is precisely the case that is required to investigate collisions of atoms in rf-dressed traps. Owens *et al.* [13] have shown that rf dressing can be used to create new Feshbach resonances at desired magnetic fields

that are convenient for atomic cooling. These resonances may be valuable for molecule formation, particularly in heteronuclear systems.

Most experimental work with rf-dressed traps to date has used ^{87}Rb atoms. However, there is considerable interest in extending this to other atomic species. In this paper we use coupled-channel calculations to explore the rates of rf-induced inelastic collisions theoretically. We show that ^{87}Rb is a special case, where the losses induced by rf radiation are very small. Most other alkali-metal atoms may be expected to have much faster rf-induced collisional losses.

II. METHODS

We use the convention that lower-case quantum numbers refer to individual atoms and upper-case quantum numbers refer to the colliding pair. In the absence of fields, each atom is described by its electron spin $s = 1/2$ and nuclear spin i , which couple to form a resultant f . In a magnetic field B , each state splits into components labeled by $m_f = m_s + m_i$, where each m is the projection of the corresponding quantity on the magnetic field axis Z . The Hamiltonian for each atom is

$$\hat{h} = \zeta \hat{i} \cdot \hat{s} + (g_S \hat{s}_z + g_i \hat{i}_z) \mu_B B, \quad (1)$$

where ζ is the hyperfine coupling constant and g_S and g_i are electron and nuclear spin g -factors with the sign convention of Arimondo *et al.* [14]. At the low magnetic fields considered here, f is nearly conserved but m_s and m_i are not.

To incorporate the effects of rf radiation on a single atom, we use a basis set of photon-dressed functions in an uncoupled representation, $|sm_s\rangle|im_i\rangle|NM_N\rangle$, where N is the photon number with respect to the average photon number N_0 . In the present work we focus on circularly polarized radiation, with either $M_N = N$

* Author to whom correspondence should be addressed:
j.m.hutson@durham.ac.uk

(right-circularly polarized, σ_+) or $M_N = -N$ (left-circularly polarized, σ_-). In the present work we consider σ_- polarization, with $\mathbf{B}(t) = B_{\text{rf}}[\hat{e}_x \cos 2\pi\nu t - \hat{e}_y \sin 2\pi\nu t]$, where \hat{e}_x and \hat{e}_y are unit vectors along the X and Y axes. The Hamiltonian of the rf field is

$$\hat{h}_{\text{rf}} = h\nu(\hat{a}_-^\dagger \hat{a}_- - N_0), \quad (2)$$

where \hat{a}_- and \hat{a}_-^\dagger are photon annihilation and creation operators for σ_- photons. Its interaction with an atom is

$$\hat{h}_{\text{rf}}^{\text{int}} = \frac{\mu_B B_{\text{rf}}}{2\sqrt{N_0}} \left[(g_S \hat{s}_+ + g_I \hat{i}_+) \hat{a}_-^\dagger + (g_S \hat{s}_- + g_I \hat{i}_-) \hat{a}_- \right], \quad (3)$$

where B_{rf} is the amplitude of the oscillating magnetic field, \hat{s}_+ and \hat{s}_- are raising and lowering operators for the electron spin and \hat{i}_+ and \hat{i}_- are the corresponding operators for the nuclear spin. For σ_+ polarization, \hat{a}_+ replaces \hat{a}_-^\dagger and \hat{a}_+^\dagger replaces \hat{a}_- in Eq. (3). For σ_X radiation with rf field $\mathbf{B}(t) = B_{\text{rf}} \cos 2\pi\nu t$, both σ_+ and σ_- coupling terms are present, renormalized by 1/2 [15].

If couplings involving the photon annihilation and creation operators are neglected, states with different m_f values and different photon numbers N cross as a function of magnetic field. For example, for ^{87}Rb , with $i = 3/2$, and 3.0 MHz radiation, the $(f, m_f, N) = (1, +1, 1)$, $(1, 0, 0)$ and $(1, -1, -1)$ states all cross near $B = 4.27$ G, as shown in Fig. 1. If the radiation has σ_- polarization, these three states all have the same total projection quantum number $M_{\text{tot}}^{\text{atom}}$, and are coupled by the interaction (3), so the triple crossing becomes an avoided crossing; for $B_{\text{rf}} = 0.5$ G, the minimum separation between the states is $h \times 0.35$ MHz. Ultracold atoms in the uppermost state can be trapped in the vicinity of the avoided crossing. These atoms are in a state whose character is principally $(1, +1, 1)$ on the low-field side of the crossing, but is $(1, -1, -1)$ on the high-field side and a complicated mixture of all three states close to the crossing itself.

We carry out quantum scattering calculations of collisions between pairs of atoms in rf-dressed states. The Hamiltonian for the colliding pair is

$$\frac{\hbar^2}{2\mu} \left[-R^{-1} \frac{d^2}{dR^2} R + \frac{\hat{L}^2}{R^2} \right] + \hat{V}(R) + \hat{h}_1 + \hat{h}_2 + \hat{h}_{\text{rf}} + \hat{h}_{\text{rf},1}^{\text{int}} + \hat{h}_{\text{rf},2}^{\text{int}}, \quad (4)$$

where μ is the reduced mass, \hat{L}^2 is the operator for the end-over-end angular momentum of the two atoms about one another, and $\hat{V}(R)$ is the interaction operator,

$$\hat{V}(R) = \hat{V}^c(R) + \hat{V}^d(R). \quad (5)$$

Here $\hat{V}^c(R) = V_0(R)\hat{\mathcal{P}}^{(0)} + V_1(R)\hat{\mathcal{P}}^{(1)}$ is an isotropic potential operator that depends on the electronic potential energy curves $V_0(R)$ and $V_1(R)$ for the singlet and triplet electronic states and $\hat{V}^d(R)$ is a relatively weak anisotropic operator that arises from the combination

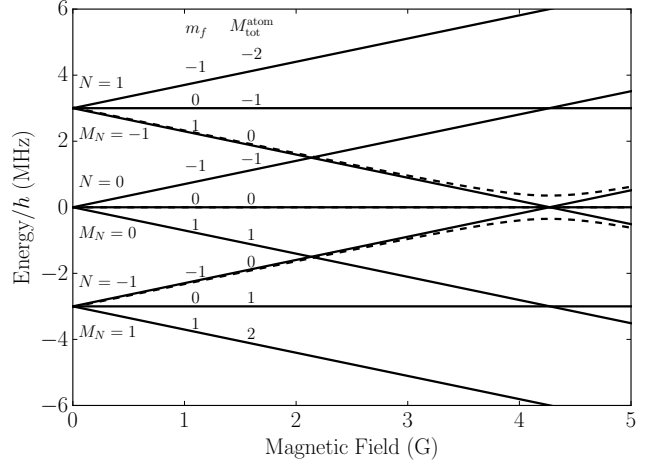


FIG. 1. rf-dressed atomic levels of $f = 1$ states of ^{87}Rb for frequency 3.0 MHz and photon numbers $N = -1, 0$ and 1 , shown with respect to the energy of the $f = 1, m_f = 0$ state for $N = 0$. Solid lines show levels for zero rf intensity and dashed curves show levels for $B_{\text{rf}} = 0.5$ G with $M_{\text{tot}}^{\text{atom}} = 0$. Atoms can be trapped at the minimum in the upper dashed curve.

of spin dipolar coupling at long range and second-order spin-orbit coupling at short range. The singlet and triplet projectors $\hat{\mathcal{P}}^{(0)}$ and $\hat{\mathcal{P}}^{(1)}$ project onto subspaces with total electron spin quantum numbers 0 and 1 respectively. The potential curves for the singlet and triplet states are taken from ref. [16] for Rb_2 and from ref. [17] for K_2 .

The basis set of photon-dressed functions for a pair of atoms is

$$|s_1 m_{s1}\rangle |i_1 m_{i1}\rangle |s_2 m_{s2}\rangle |i_2 m_{i2}\rangle |LM_L\rangle |NM_N\rangle, \quad (6)$$

where L is the angular momentum for relative motion and M_L is its projection onto Z . The basis set is symmetrized to take account of exchange symmetry. The matrix elements of the Hamiltonian in this basis set have been given in the Appendix of ref. [18], except for the rf terms, which involve raising and lowering operators with non-zero matrix elements

$$\langle sm_s \pm 1 | \hat{s}_\pm | sm_s \rangle = [s(s+1) - m_s(m_s \pm 1)]^{\frac{1}{2}}; \quad (7)$$

$$\langle im_i \pm 1 | \hat{i}_\pm | im_i \rangle = [i(i+1) - m_i(m_i \pm 1)]^{\frac{1}{2}} \quad (8)$$

and photon creation and annihilation operators with non-zero matrix elements

$$\langle N + 1 M_N \pm 1 | \hat{a}_\pm^\dagger | NM_N \rangle = (N_0 + N + 1)^{\frac{1}{2}}; \quad (9)$$

$$\langle N - 1 M_N \mp 1 | \hat{a}_\pm | NM_N \rangle = (N_0 + N)^{\frac{1}{2}}; \quad (10)$$

$$\langle NM_N | \hat{a}_\pm^\dagger \hat{a}_\pm | NM_N \rangle = N_0 + N. \quad (11)$$

We assume $N_0 \gg N$, so that the matrix elements of \hat{a}_\pm^\dagger and \hat{a}_\pm cancel with the factor $N_0^{1/2}$ in the denominator of Eq. (3).

The only conserved quantum numbers in a collision are parity $(-1)^L$ and the total projection $M_{\text{tot}} = M_F + M_L + M_N$, where $M_F = m_{f1} + m_{f2}$. Our basis set includes all possible values of m_{s1} , m_{s2} , m_{i1} , m_{i2} and M_L , for each value of L and M_N that give the required parity and M_{tot} . The values of L , N and M_N are limited by $L \leq L_{\text{max}}$, $|N| \leq N_{\text{max}}$ and $|M_N| \leq N_{\text{max}}$; the values used for L_{max} and N_{max} will be described for each set of calculations.

Expanding the scattering wavefunction in the basis set described above produces a set of coupled equations in the interatomic distance coordinate R . The number of coupled equations varies from 30 to 208. These equations are solved using the MOLSCAT package [19]. In the present work we use the hybrid log-derivative propagator [20] to propagate the coupled equations from short range out to $R_{\text{max}} = 15,000$ bohr. MOLSCAT applies scattering boundary conditions to extract the scattering S matrix, and then obtains the complex energy-dependent scattering length $a(E, B) = \alpha(E, B) - i\beta(E, B)$ from the identity [21]

$$a(E, B) = \frac{1}{ik} \left(\frac{1 - S_{00}(E, B)}{1 + S_{00}(E, B)} \right), \quad (12)$$

where $k^2 = 2\mu E/\hbar^2$ and $S_{00}(E, B)$ is the diagonal S -matrix element in the incoming s-wave channel. This is constant as $E \rightarrow 0$, where it reduces to the usual zero-energy scattering length in the absence of inelastic collisions. For s-wave collisions (incoming $L = 0$), the rate coefficient for inelastic loss is [22]

$$k_2(E, B) = \frac{2\hbar g_\alpha \beta(E, B)}{\mu [1 + k^2 |a(E, B)|^2 + 2k\beta(E, B)]}, \quad (13)$$

where g_α is 2 for identical bosons and 1 for distinguishable particles. This is independent of energy in the limit $E \rightarrow 0$, but resonant peaks are moderated by the $k^2 |a|^2$ term in the denominator at the collision energy of $1 \mu\text{K} \times k_B$ used in the present calculations.

III. RESULTS

In this section we present the results of coupled-channel scattering calculations for rf-dressed states of ^{39}K and ^{87}Rb in the vicinity of an rf-dressed trap. Since ^{87}Rb is a special case with highly atypical properties, we consider first the more typical case of ^{39}K , which (like ^{87}Rb) has nuclear spin $i = 3/2$ and a hyperfine ground state with $f = 1$.

To describe an rf-dressed trap for $f = 1$ atoms requires a minimum of 3 rf-free states with $(f, m_f, N) = (1, +1, 1)$, $(1, 0, 0)$ and $(1, -1, -1)$, as shown in Fig. 1. To describe a *pair* of such states requires photon numbers N from -2 to 2 . For rf field amplitude $B_{\text{rf}} = 0.5$ G, this produces atomic collision thresholds as shown for $^{87}\text{Rb} + ^{87}\text{Rb}$ in Fig. 2. The thresholds for $^{39}\text{K} + ^{39}\text{K}$ are

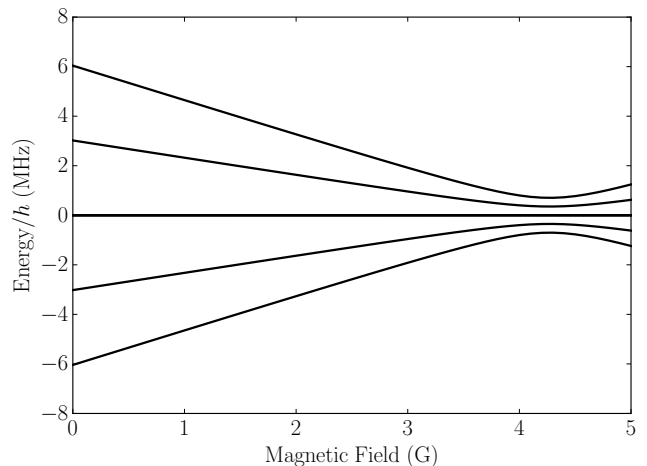


FIG. 2. The rf-dressed atomic thresholds of $^{87}\text{Rb} + ^{87}\text{Rb}$ for $f = 1$ and $M_{\text{tot}} = 0$. The corresponding thresholds of $^{39}\text{K} + ^{39}\text{K}$ are almost identical. The rf-induced collisions that cause trap loss are from the uppermost of these thresholds to all the lower ones. The thresholds are calculated for $\nu = 3.0$ MHz and $B_{\text{rf}} = 0.5$ G. Near zero magnetic field the thresholds can be labeled from top to bottom as $M_F = -2, -1, 0, +1, +2$ with $N = -2, -1, 0, +1, +2$, respectively.

almost identical. Pairs of atoms are trapped at the highest of the 5 thresholds shown, and can undergo inelastic collisions to produce atoms at the lower thresholds. Such inelastic collisions release kinetic energy of at least $\hbar \times 0.25 \text{ MHz} \approx k_B \times 12.5 \mu\text{K}$, and the recoil will usually eject both collision partners from the trap.

A. Inelastic collisions of rf-dressed ^{39}K

The inelastic collision rates for $^{39}\text{K} + ^{39}\text{K}$ at $B_{\text{rf}} = 0.5$ G are shown in Fig. 3(a), as a function of magnetic field across the trap. The solid line shows the inelastic rate from calculations with $L_{\text{max}} = 2$, while the dashed line shows the rate from simplified (and computationally far cheaper) calculations with $L_{\text{max}} = 0$. Both calculations use photon numbers $-2 \leq N \leq 2$, and adding additional values of N makes no further difference to the results.

The main source of inelasticity in $^{39}\text{K} + ^{39}\text{K}$ collision exists even for $L_{\text{max}} = 0$. It arises from collisions that conserve $m_{f1} + m_{f2} + M_N$ and thus do not change M_L ; we refer to these as rf-induced collisions. Since L does not need to change, there is no centrifugal barrier in the outgoing channel and no centrifugal suppression of the inelastic rate. For $B_{\text{rf}} = 0.5$ G, the loss rate peaks at $k_2^{\text{max}} = 6.33 \times 10^{-14} \text{ cm}^3 \text{ s}^{-1}$ ($\beta = 0.015$ bohr) near the trap center and dies off on either side. However, the peak is a strong function of B_{rf} . Figure 4 shows the height k_2^{max} and full width at half maximum (FWHM) of the peak as a function of B_{rf} , obtained from calculations with $L_{\text{max}} = 0$; the peak width increases as B_{rf} increases, but the peak height decreases. The width increases faster

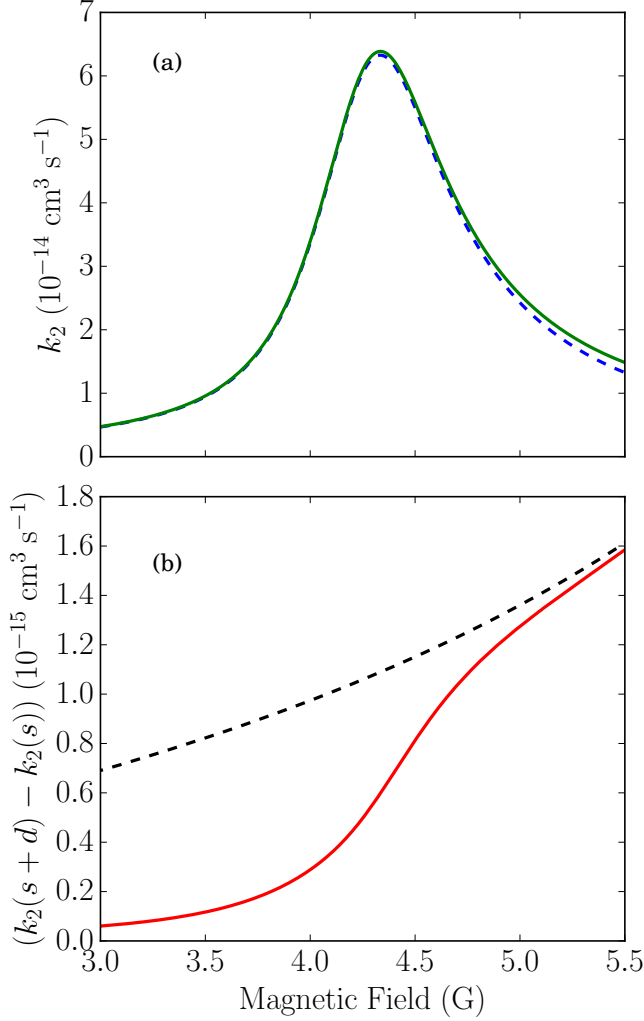


FIG. 3. (a) Rate coefficient for inelastic loss of adiabatically trapped $^{39}\text{K}+^{39}\text{K}$ as a function of magnetic field with $\nu = 3.0$ MHz and $B_{\text{rf}} = 0.5$ G, from calculations with $L_{\text{max}} = 2$ (solid, green) and $L_{\text{max}} = 0$ (dashed, blue). (b) Contribution from rf-modified spin-relaxation collisions, obtained from the difference between the $L_{\text{max}} = 0$ and $L_{\text{max}} = 2$ results (red, solid) compared with rf-free spin-relaxation for $(f, m_f) = (1, -1)$ atoms (black, dashed).

than linearly with B_{rf} ; although the range of B across which the atomic states are strongly mixed by rf dressing is linear in B_{rf} , the kinetic energy released also depends on B_{rf} and this affects the inelastic cross sections in a complicated way. The peak cross section decreases as the kinetic energy release increases.

For $^{39}\text{K}+^{39}\text{K}$, the inelastic rates are fairly similar for $L_{\text{max}} = 2$ and $L_{\text{max}} = 0$. The small difference arises because, even in the absence of rf radiation, atoms in $f = 1, m_f < 1$ may undergo spin-relaxation collisions to produce atoms in lower magnetic sublevels. Such collisions are driven only by the weak anisotropic part of the interaction, $V^d(R)$ in Eq. (5). Since they change $M_F = m_{f1} + m_{f2}$, and $M_F + M_L$ must be conserved,

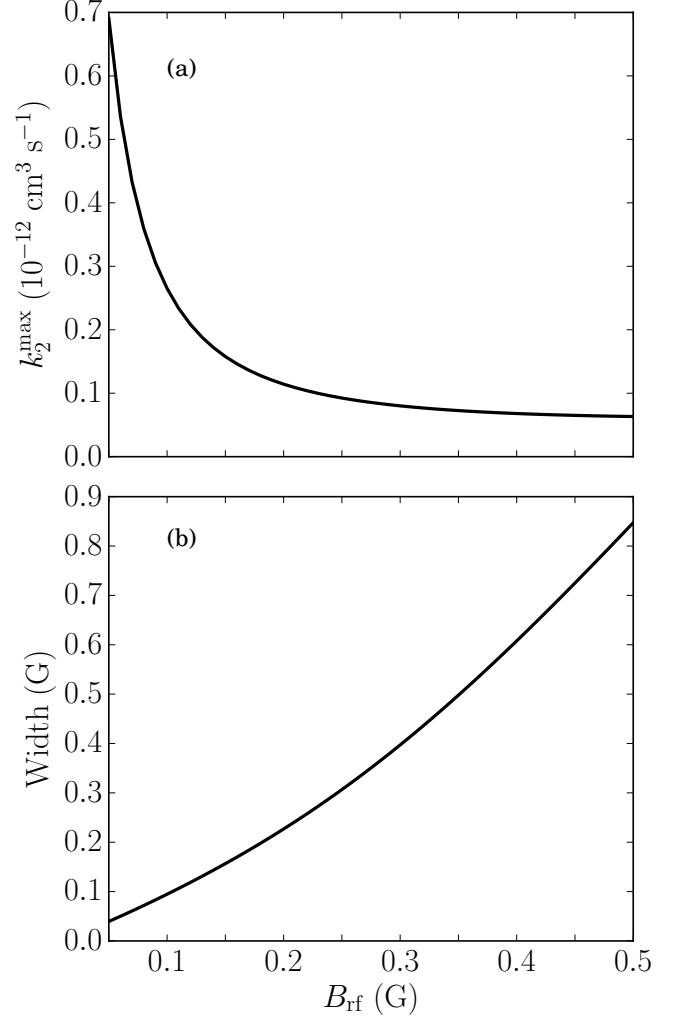


FIG. 4. Height and FWHM width of the peak in inelastic rate coefficient for $^{39}\text{K}+^{39}\text{K}$, as a function of rf amplitude B_{rf} .

they must also change M_L . For s-wave collisions, L is initially zero, so changing M_L requires a final state with $L > 0$, which must have $L \geq 2$ to conserve parity. The rates of spin-relaxation collisions are therefore suppressed because the products are trapped inside an $L = 2$ centrifugal barrier, which has height $k_B \times 1.5$ mK for $^{39}\text{K}+^{39}\text{K}$. Figure 3(b) shows the *difference* between the $L_{\text{max}} = 2$ and $L_{\text{max}} = 0$ results in Fig. 3(a) and compares it with the rate of spin-relaxation collisions from an rf-free calculation for two atoms initially in the $(f, m_f) = (1, -1)$ state. It may be seen that the difference approaches the rf-free spin-relaxation rate at high magnetic field, where the adiabatically trapped state is principally $(1, -1)$. However, it decreases to zero at low magnetic field, where the trapped state is principally $(1, 1)$, which is the rf-free ground state and cannot undergo inelastic collisions. At the trap center the rf-modified spin-relaxation rate is about half its rf-free value.

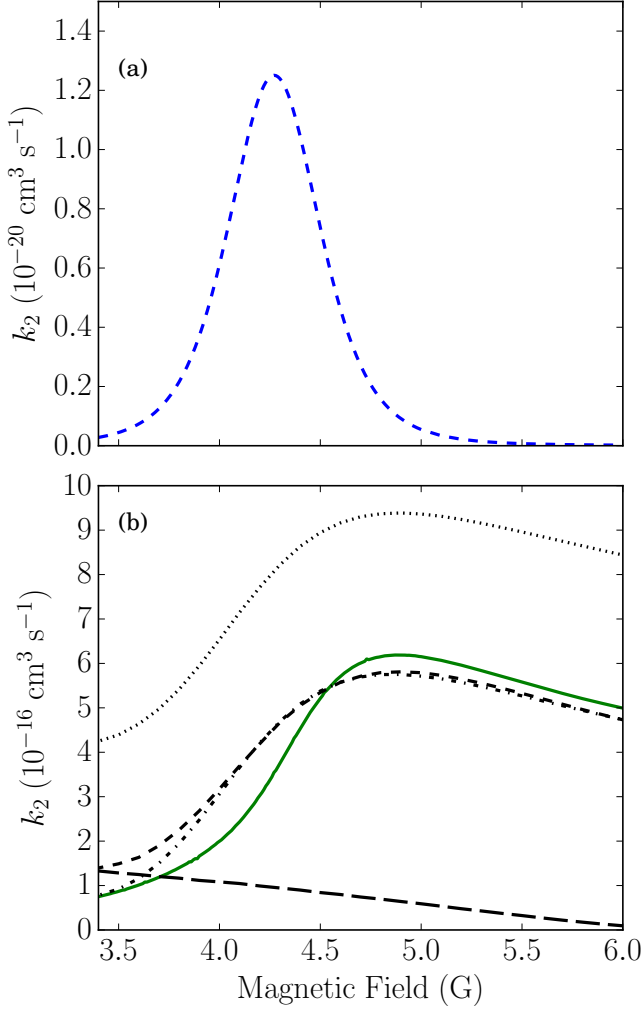


FIG. 5. Rate coefficient for inelastic loss for adiabatically trapped ^{87}Rb in $f = 1$ as a function of magnetic field with $\nu = 3.0$ MHz and $B_{\text{rf}} = 0.5$ G. (a) Calculation using $L_{\text{max}} = 0$. (b) Calculation including spin relaxation, using $L_{\text{max}} = 2$ (solid green line). Rate coefficients for rf-free spin relaxation are shown as dashed lines for $(1, -1) + (1, -1)$, dashed-dotted lines for $(1, -1) + (1, 0)$, dotted lines for $(1, 0) + (1, 0)$ and long dashed lines for $(1, 0) + (1, 1)$.

B. Inelastic collisions of rf-dressed ^{87}Rb

Figure 5 show the calculated inelastic rate constant as a function of magnetic field for ^{87}Rb , for the same rf frequency and field strength as Fig. 3. Figures 5(a) and 5(b) show calculations with $L_{\text{max}} = 0$ and 2, respectively. In this case the rate coefficient for rf-induced loss (with $L_{\text{max}} = 0$) reaches a maximum of only $k_2^{\text{max}} = 1.25 \times 10^{-20} \text{ cm}^3 \text{ s}^{-1}$ ($\beta = 6.47 \times 10^{-8}$ bohr) at $B = 4.2713$ G (the trap center). This is more than 6 orders of magnitude slower than for $^{39}\text{K}_2$, and 4 orders of magnitude lower than the rf-modified spin-relaxation rate at the trap center. Consequently Fig. 5(b) is totally dominated by spin relaxation. In this case, however, the spin

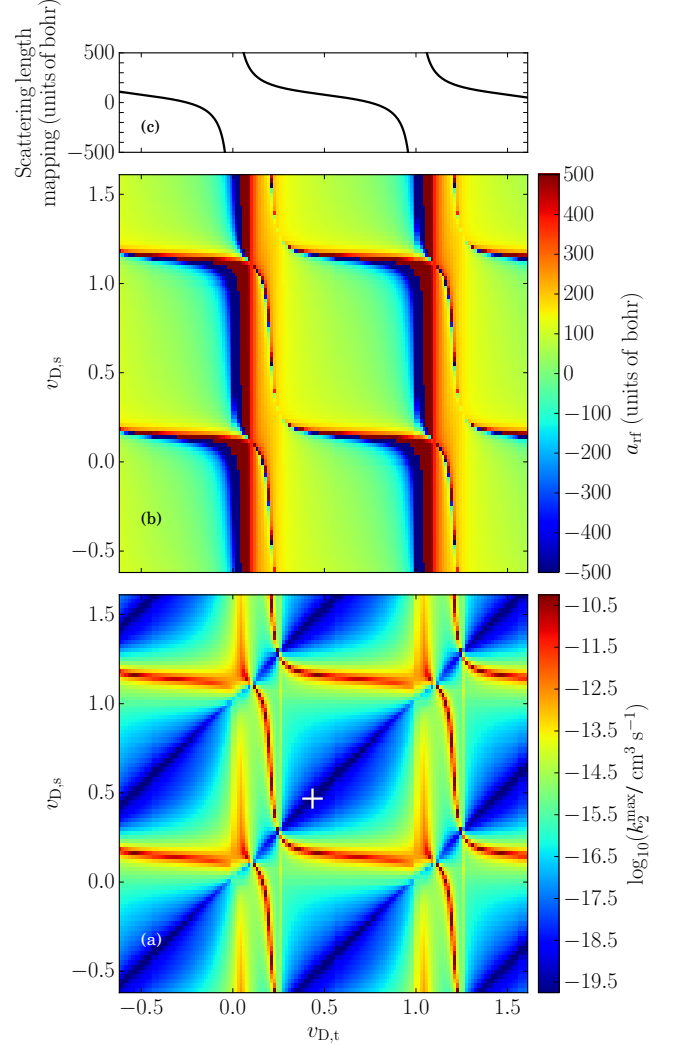


FIG. 6. Contour plots of the dependence of collision properties on the fractional part of v_D for the singlet and triplet states, for adiabatically trapped ^{87}Rb in $f = 1$ with $\nu = 3.0$ MHz and $B_{\text{rf}} = 0.5$ G. (a) Rate coefficient for rf-induced loss at the trap center, k_2^{max} ; (b) Real part of scattering length a_{rf} . (c) Mapping between v_D and the singlet and triplet scattering lengths for ^{87}Rb , according to Eq. 14.

relaxation itself shows more complicated structure as a function of B ; the dashed lines in Fig. 3(b) show the rf-free spin relaxation rates for $(1, 1) + (1, 1)$, $(1, 1) + (1, 0)$, $(1, 1) + (1, -1)$ and $(1, 0) + (1, -1)$ collisions. As for ^{39}K , the losses for rf-dressed states approach those for rf-free $(1, 1) + (1, 1)$ at high magnetic field, but around the trap centre there are also contributions from other components of the wavefunction of the rf-dressed atomic states.

The rf-induced loss rate depends strongly on the singlet and triplet scattering lengths a_s and a_t . In order to explore this, we have carried out $L_{\text{max}} = 0$ calculations on a set of potentials modified at short range to allow adjustment of a_s and a_t . We retained the functional forms of the potential curves of Strauss *et al.* [16], but modi-

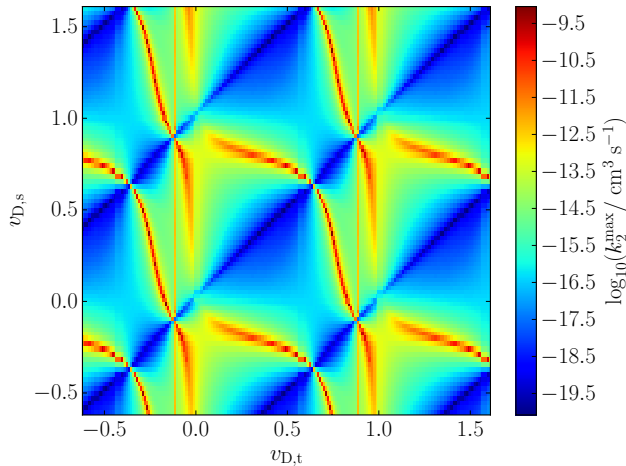


FIG. 7. Contour plot of the rate coefficient for rf-induced loss at the trap center, for adiabatically trapped $f = 1$ states of an artificial atom with a hyperfine splitting 0.7 times that of ^{87}Rb . All other quantities are the same as for Fig. 6.

fied the short-range matching point R_{SR} to 3.5 Å for the singlet potential and to 5.6 Å for the triplet potential in order to provide sufficient flexibility to adjust the scattering lengths through a complete cycle. We then adjusted the short-range power N_{SR} to obtain modified potentials with different scattering lengths, maintaining continuity of the potential and its derivative at R_{SR} as described in ref. [23].

Contour plots of the resulting rf-induced peak loss rates k_2^{max} and the corresponding real part of the scattering length a_{rf} (for collisions of rf-dressed atoms) are shown in Figure 6, calculated at the trap center for $B_{\text{rf}} = 0.5$ G. Since the possible singlet and triplet scattering lengths range from $-\infty$ to $+\infty$, the loss rate is displayed as a function of two phases, defined as the fractional parts of the quantum numbers at dissociation $v_{D,s}$ and $v_{D,t}$ for the singlet and triplet states. These each map onto the corresponding scattering length according to

$$a = \bar{a} \left[1 - \tan \left(v_D + \frac{1}{2} \right) \pi \right], \quad (14)$$

where $\bar{a} = 0.477988 \dots (2\mu C_6/\hbar^2)^{-1/4}$ is the mean scattering length of Gribakin and Flambaum [24] and C_6 is the leading long-range dispersion coefficient. For ^{87}Rb , $\bar{a} = 78.95$ bohr. The mapping between scattering length and v_D is shown for ^{87}Rb in the top panel of Fig. 6.

Figure 6 shows that k_2^{max} varies by more than 10 orders of magnitude as a function of the singlet and triplet scattering lengths. Both k_2^{max} and a_{rf} depend only on the fractional parts of v_D for the singlet and triplet states (and hence on a_s and a_t), as indicated by the repeating patterns in Fig. 6. The most striking feature of Fig. 6(a) is a deep diagonal trough in the rf-induced loss rate when $v_{D,s} \approx v_{D,t}$ ($a_s \approx a_t$), with no corresponding feature in a_{rf} . Superimposed on this are peaks in k_2^{max} and poles in

the corresponding a_{rf} . These are of three different types. First, there are near-vertical bands near integer values of $v_{D,t}$, corresponding to $|a_t| = \infty$. These are entrance-channel resonances; they occur near integer values of $v_{D,t}$ because the incoming channel is mostly triplet in character. Secondly, there is a Feshbach resonance due to a closed channel with excited hyperfine character ($f = 2$ here), which produces curving bands of peaks in k_2^{max} that cross the vertical bands near $v_{D,s} \approx 0.1$. Lastly, there is an additional Feshbach resonance that produces very narrow vertical bands of peaks near $v_{D,t} \approx 0.3$; these probably arise from pure triplet states that exist at the $(f_1, f_2) = (1, 2)$ threshold in the absence of rf and magnetic fields.

To explore the dependence of the pattern on hyperfine splitting, we have repeated the calculations on a series of artificial systems with the ^{87}Rb hyperfine splitting reduced from its real value, using the same set of interaction potentials. The results with the hyperfine splitting at 70% of its real value are shown in Fig. 7. The general form of the contour plot is unchanged, with a deep trough around $v_{D,s} \approx v_{D,t}$ ($a_s \approx a_t$) and peaks around vertical bands at integer values of $v_{D,t}$. As expected, however, the Feshbach peaks have shifted. They now display distinct *avoided* crossings with the vertical bands of peaks. For some values of the hyperfine splitting, the crossings are so strongly avoided that the vertical bands near integer $v_{D,t}$ are barely identifiable.

The trough observed here for rf-induced inelastic collisions when $a_s \approx a_t$ has a similar origin to that found for spin-exchange collisions. Myatt *et al.* [25] measured a very low rf-free spin-exchange rate in dual Bose-Einstein condensates of ^{87}Rb in $(f, m_f) = (1, -1)$ and $(2, 2)$ states. Julienne *et al.* [26] explained this using an adiabatic model of the collision dynamics [27] where the Hamiltonian of Eq. 4 (without rf) is diagonalized at each value of the interatomic distance R . For ^{87}Rb , the exchange splitting between the singlet and triplet curves is comparable to the hyperfine splitting around $R_X = 22$ bohr. Inside this distance the adiabatic states are essentially pure singlet and triplet states, whereas outside it they are described by atomic quantum numbers (f, m_f) . Julienne *et al.* [26] considered scattering at zero magnetic field, with f_1 and f_2 coupled to give a resultant F . The resulting rf-free adiabats for $F = 2$ are shown in Fig. 8(a), with respect to the pure triplet interaction potential. The nonadiabatic matrix elements $\langle i | d/dR | j \rangle$ between the states that are asymptotically $(f_1, f_2, F) = (1, 1, 2)$, $(1, 2, 2)$ and $(2, 2, 2)$ are shown in Fig. 8(c). The overall magnitude is usefully characterized by the integral

$$D_{ij} = \int \left\langle i \left| \frac{d}{dR} \right| j \right\rangle dR, \quad (15)$$

which is $\pi/2$ for a complete avoided crossing, and 1.05, 0.55 and 0.49 for the three couplings in Fig. 8(c). The adiabats and nonadiabatic couplings are independent of the singlet and triplet scattering lengths. However, Julienne *et al.* [26] argued that, when $a_s \approx a_t$, the radial

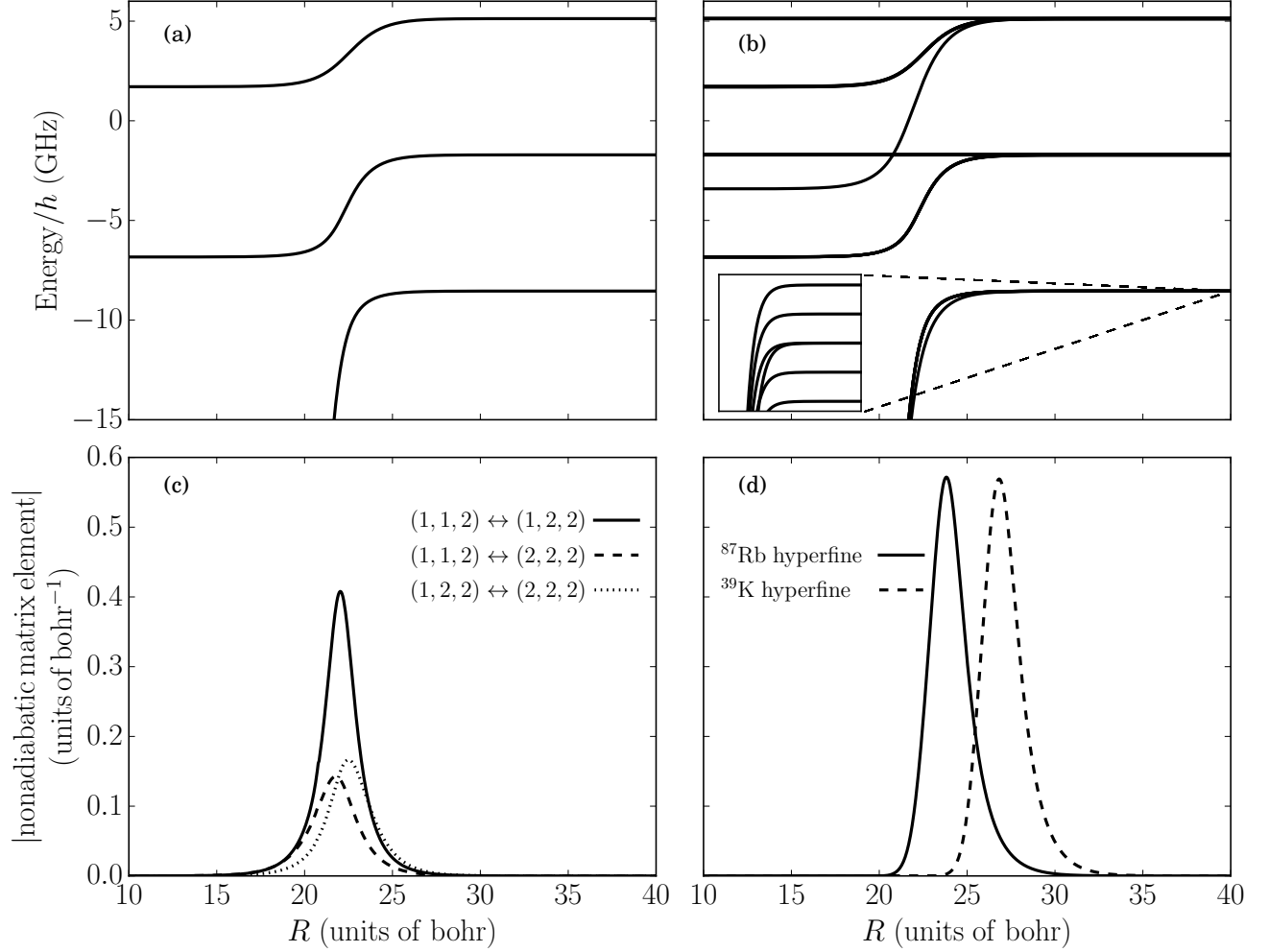


FIG. 8. Adiabats (eigenvalues of the Hamiltonian of Eq. 4 at fixed R) with respect to a pure triplet curve (a) for field-free collisions with $(f_1, f_2, F = 2)$; (b) for collisions of rf-dressed atoms with $f = 1$, at the trap center with rf field frequency 3 MHz and strength $B_{\text{rf}} = 0.5$ G, for $M_{\text{tot}} = 0$. (c) nonadiabatic matrix elements between $(1,1,2)$, $(1,2,2)$ and $(2,2,2)$ in (a); (d) nonadiabatic matrix element between the uppermost of the six $(f_1, f_2, M_{\text{tot}}) = (1, 1, 0)$ rf-dressed states and the next-highest state.

wavefunctions $R^{-1}\chi_i(R)$ and $R^{-1}\chi_j(R)$ in the incoming $(1,2,2)$ and inelastic outgoing $(1,1,2)$ channels are in phase around R_X . This minimizes the matrix element that controls inelastic scattering,

$$-\frac{\hbar^2}{2\mu} \int \chi_i(R)^* \left\langle i \left| \frac{d}{dR} \right| j \right\rangle \frac{d}{dR} \chi_j(R) dR. \quad (16)$$

Figures 8(a) and (c) may be compared with the adiabats for collisions of rf-dressed ^{87}Rb atoms in $f = 1$ states at the trap center (4.27 G), which are shown in Fig. 8(b), and the nonadiabatic matrix element from the uppermost of the six $(f_1, f_2, M_{\text{tot}}) = (1, 1, 0)$ states to the next-highest state, which are shown in Fig. 8(d). The nonadiabatic matrix element again peaks around 22 bohr for ^{87}Rb ; the mechanism is similar to that for spin exchange, and the overall inelastic coupling is smallest when $a_s \approx a_t$, producing the diagonal troughs seen in Figs. 6 and 7.

The actual singlet and triplet scattering lengths for ^{87}Rb are indicated by a cross on Fig. 6(a). This shows that ^{87}Rb is special in two different ways. Not only are its singlet and triplet scattering lengths quite similar, but their actual values correspond to $v_D \approx 0.5$ and lie well away from the peaks due to Feshbach resonances. The value of k_2^{max} at the deepest point in the trough in Fig. 6(a) is about $k_2^{\text{max}} = 3.6 \times 10^{-20} \text{ cm}^3 \text{ s}^{-1}$, which is not far from the value of $1.25 \times 10^{-20} \text{ cm}^3 \text{ s}^{-1}$ obtained for ^{87}Rb on the potentials of ref. [16].

Figure 9 shows a contour plot similar to Fig. 7 but with the hyperfine splitting of ^{39}K (462 MHz). The structure is similar, with a Feshbach resonance avoided-crossing with vertical bands of peaks at integer $v_{D,t}$, though the resonances are distinctly wider than in Figs. 6(a) and 7. The actual scattering lengths of ^{39}K are shown as a black cross; the value of k_2^{max} at this point is $5.3 \times 10^{-14} \text{ cm}^3 \text{ s}^{-1}$, which may be compared with $k_2^{\text{max}} = 6.33 \times$

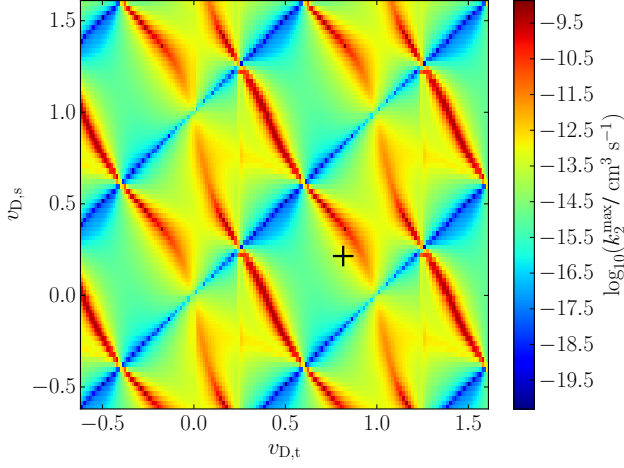


FIG. 9. Contour plot of the rate coefficient for rf-induced loss at the trap center, for adiabatically trapped $f = 1$ states of an artificial atom with the mass of ^{87}Rb with the hyperfine splitting of ^{39}K . All other quantities are the same as for Fig. 6.

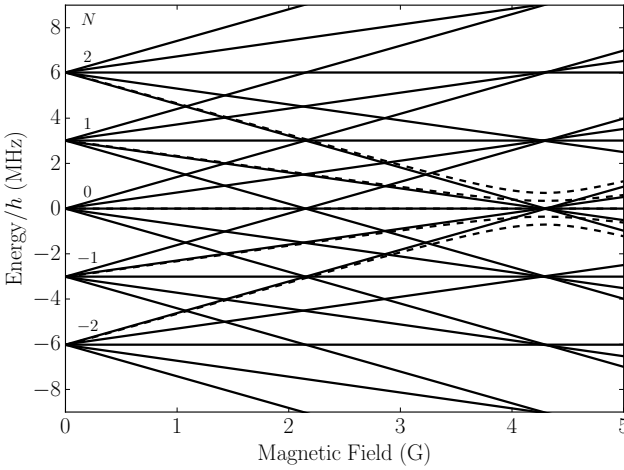


FIG. 10. rf-dressed atomic levels of $f = 2$ states of ^{87}Rb for frequency 3.0 MHz and photon numbers $N = -2, -1, 0, 1$ and 2 , shown with respect to the energy of the $f = 2$, $m_f = 0$ state for $N = 0$. Solid lines show levels for zero rf intensity and dashed lines show levels for $B_{\text{rf}} = 0.5$ G with $M_{\text{tot}} = 0$. Atoms can be trapped at the minimum in the uppermost dashed curve.

$10^{-14} \text{ cm}^3 \text{s}^{-1}$ from the calculation with the mass and interaction potentials for ^{39}K in section III A.

C. Inelastic collisions of rf-dressed $f = 2$ states

A somewhat different case occurs for atoms in $f = 2$ states. Here there are 5 photon-dressed atomic states that cross as a function of magnetic field, as shown for ^{87}Rb in Fig. 10. It requires a minimum of 5 rf-free states

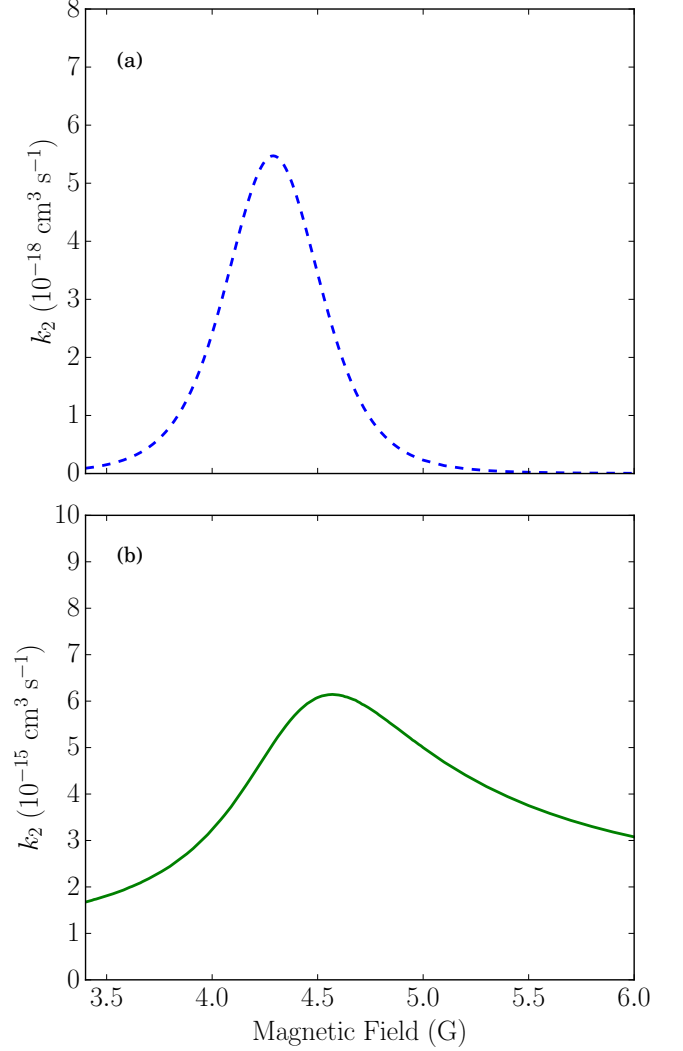


FIG. 11. Rate coefficient for inelastic loss of adiabatically trapped ^{87}Rb in $f = 2$ as a function of magnetic field with $\nu = 3.0$ MHz and $B_{\text{rf}} = 0.5$ G. (a) Calculation of rf-induced loss, using $L_{\text{max}} = 0$. (b) Calculation including spin relaxation, using $L_{\text{max}} = 2$.

(with photon numbers N from -2 to 2) to describe a single trapped atom, and describing two such atoms requires photon numbers from -4 to 4 . The coupled-channel calculation is thus computationally considerably more expensive. Nevertheless, the principles are exactly the same and rate coefficients for inelastic loss can again be obtained from β , the imaginary part of the complex scattering length, for atoms initially at the highest rf-dressed threshold.

Figure 11 shows the rate coefficient for inelastic loss for ^{87}Rb in $f = 2$, as a function of magnetic field near the trap center. As before, Fig. 11(a) shows the rf-induced loss, from a calculation with $L_{\text{max}} = 0$, while Fig. 11(b) shows the loss including spin relaxation, from a calculation with $L_{\text{max}} = 2$. The rf-induced loss rate is about a factor of 400 larger than for ^{87}Rb in $f = 1$, but it is

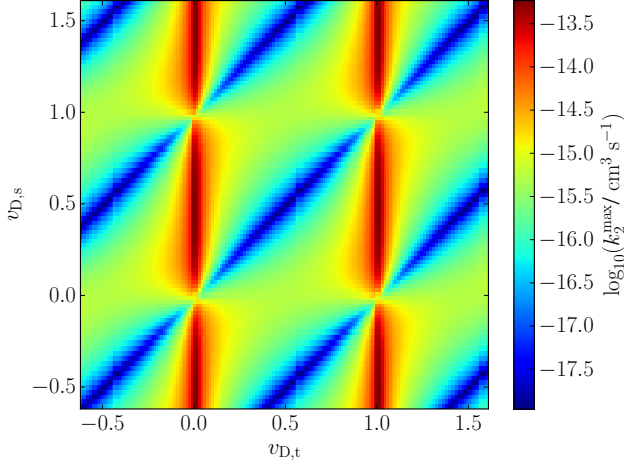


FIG. 12. Contour plot of the rate coefficient for rf-induced loss at the trap center, for adiabatically trapped $f = 2$ states of ^{87}Rb . All other quantities are the same as for Fig. 6.

still much lower than the loss rate due to spin relaxation. Once again this illustrates the special properties of ^{87}Rb .

It is notable that the rf-induced loss rate for $f = 2$ is far lower than the rf-free spin-exchange rates for $(2,0)+(2,0)$ and $(2,1)+(2,-1)$ collisions, which are 1.73×10^{-13} and $1.25 \times 10^{-13} \text{ cm}^3 \text{ s}^{-1}$ respectively. This is true even though the wavefunction for the rf-dressed atomic state includes substantial amounts of $(2,0)$ and $(2,1)$ near the trap center. It may be again rationalized by considering adiabatic curves obtained by diagonalizing the Hamiltonian of Eq. 4 at each value of the interatomic distance R . For rf-free collisions of two $f = 2$ atoms, there are contributions from $F = 0, 2$ and 4 . The inelasticity is dominated by $F = 2$, for which the adiabats and nonadiabatic matrix elements were shown in Fig. 8(a) and (c). Figure 13(a) shows the adiabats for collisions of rf-dressed ^{87}Rb atoms in $f = 2$ states at the trap center, and Fig. 13(b) shows the corresponding nonadiabatic matrix elements between the uppermost and next-highest state. The nonadiabatic coupling is quite different from the previous cases: there is no feature around 22 bohr, and instead the matrix element peaks around 32 bohr, where the difference between the singlet and triplet curves is comparable with the splittings Δ_{rf} due to rf dressing. The coupling is far weaker than in the cases shown in Fig. 8. The integral D_{ij} over the nonadiabatic coupling is only 1.96×10^{-6} , as compared to $\pi/2$ for a completed avoided crossing.

We have also investigated the dependence of k_2^{max} for the $f = 2$ states of $^{87}\text{Rb}_2$ on the singlet and triplet scattering lengths. The resulting contour plot is shown in Fig. 12. It has a considerably simpler structure than Figs. 6, 7 and 9, because the atoms are both in their upper hyperfine state and there are no closed channels that can cause Feshbach resonances. The only features are a diagonal trough for $v_{\text{D},s} \approx v_{\text{D},t}$ ($a_s \approx a_t$) and a near-vertical

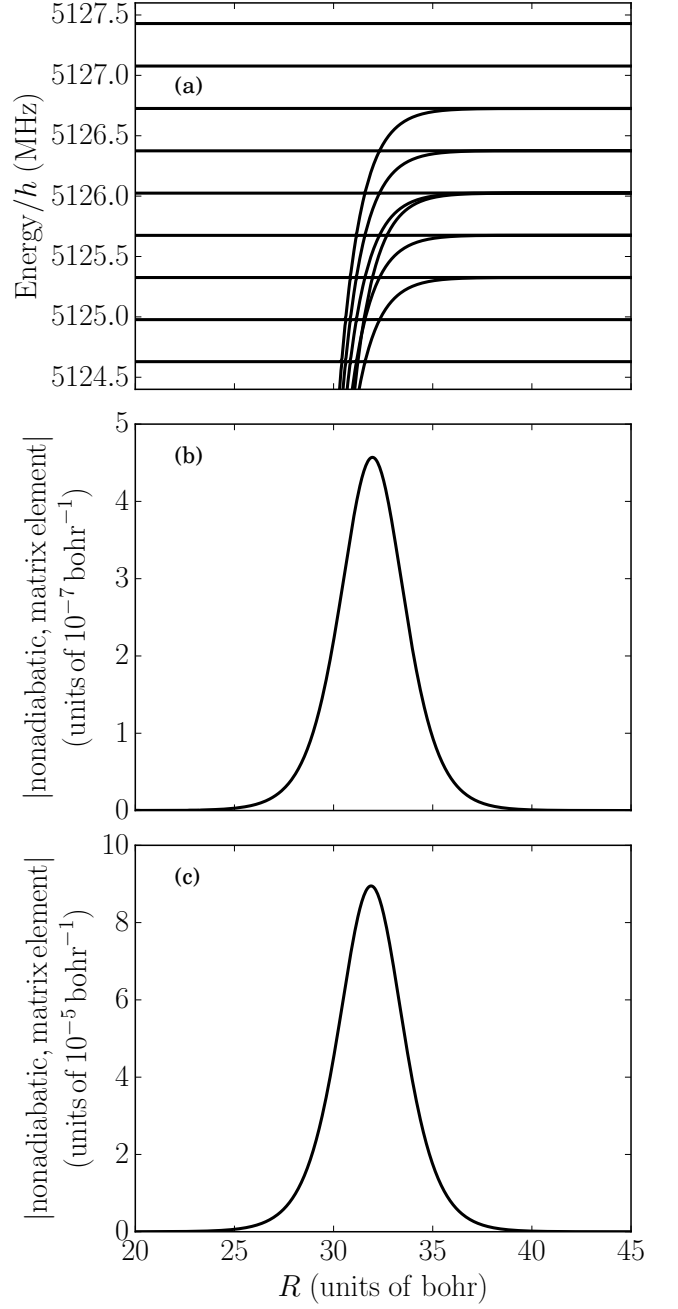


FIG. 13. (a) Adiabats (eigenvalues of the Hamiltonian of Eq. 4 at fixed R) for collisions of field-dressed ^{87}Rb atoms in $f = 2$ states, with respect to a pure triplet curve, for $M_{\text{tot}} = 0$. (b) nonadiabatic matrix elements between the top two adiabatic states for ^{87}Rb . (c) nonadiabatic matrix elements between the top two adiabatic states with the hyperfine splitting reduced to the value for ^{39}K .

band of maxima where $v_{\text{D},t}$ is close to an integer. These have the same causes as discussed for $f = 1$ above.

For atoms trapped in their upper hyperfine state, with no Feshbach resonances, the dependence of k_2^{max} on a_s and a_t may be expected to resemble Fig. 12 qualitatively for all atoms. However, there is a strong overall depen-

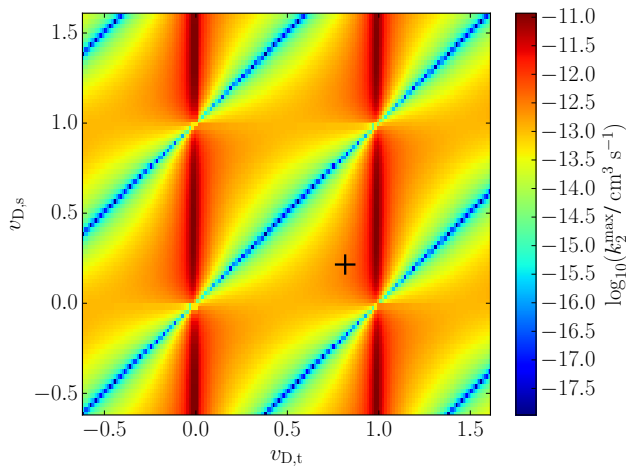


FIG. 14. Contour plot of the rate coefficient for rf-induced loss at the trap center, for adiabatically trapped $f = 2$ states of an artificial atom with the mass of ^{87}Rb but the hyperfine splitting of ^{39}K . All other quantities are the same as for Fig. 6.

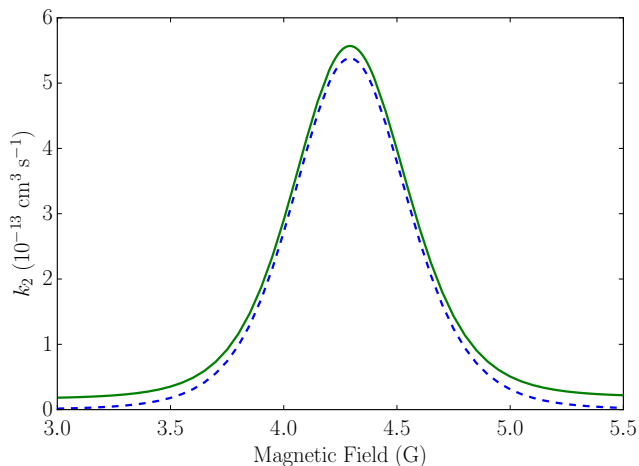


FIG. 15. Rate coefficient for inelastic loss of adiabatically trapped ^{39}K in $f = 2$ as a function of magnetic field with $\nu = 3.0$ MHz and $B_{\text{rf}} = 0.5$ G. Results are shown including spin relaxation, using $L_{\text{max}} = 2$ (solid, green) and for rf-induced loss alone, using $L_{\text{max}} = 0$ (dashed, blue).

dence on the hyperfine coupling constant. To illustrate this, we have repeated the calculations shown in Fig. 12 with the hyperfine coupling constant set to the value for ^{39}K but the reduced mass retained at the value for ^{87}Rb . The results are shown in Fig. 14. It may be seen that the general structure of peaks and troughs is unchanged, but the peaks are about a factor of 200 higher for the smaller hyperfine splitting of ^{39}K (462 MHz) than for that of ^{87}Rb (6,834 MHz). This effect may also be traced to the effects of nonadiabatic transitions. The adiabats for ^{39}K are similar to those shown for ^{87}Rb in Fig. 13(a). However, the nonadiabatic matrix element, shown in Fig.

13(c), is a factor of 200 larger than for ^{87}Rb , with integral $D_{ij} = 3.8 \times 10^{-4}$. The nonadiabatic matrix element reflects the amount of singlet character in the wavefunction of the rf-dressed atomic pair at long range; this in turn depends on the degree of mixing of $f = 1$ and $f = 2$ states in the magnetic field, which increases as the hyperfine splitting decreases.

The specific case of ^{39}K in rf-dressed $f = 2$ states is of interest. Figure 15 shows k_2 as a function of magnetic field from calculations with $L_{\text{max}} = 0$ and 2, using the potentials of ref. [17]. It may be seen that, as for ^{39}K in $f = 1$, the rf-induced loss dominates the loss due to rf-modified spin relaxation. The rate coefficient peaks at $k_2^{\text{max}} = 5.38 \times 10^{-13} \text{ cm}^3 \text{ s}^{-1}$. The rf-induced loss is about 5 orders of magnitude faster than for ^{87}Rb , and again more typical. The value is comparable to the one from Fig. 14 at the values of $v_{D,s}$ and $v_{D,t}$ for ^{39}K , shown with a black cross, which is $k_2^{\text{max}} = 2.34 \times 10^{-13} \text{ cm}^3 \text{ s}^{-1}$. The difference between these two values arises because the calculations in Fig. 14 used the reduced mass and interaction potentials for ^{87}Rb rather than ^{39}K .

An atom for which $f = 2$ is not the highest state, such as ^{85}Rb , may be expected to show more complex behavior than Fig. 12, with Feshbach resonances reappearing at some values of $v_{D,s}$ and $v_{D,t}$ (a_s and a_t). We will investigate this in future work.

IV. CONCLUSIONS

Cold atoms in radiofrequency-dressed traps may undergo inelastic collisions by mechanisms that do not occur in the absence of an rf field. These collisions may lead to trap loss. We have investigated inelastic losses for alkali-metal atoms in rf-dressed traps, using coupled-channel scattering calculations on accurate potential energy surfaces. We have explored the dependence of the loss rates on singlet and triplet scattering lengths, hyperfine splittings and the strength of the rf field.

There are two components of the inelastic loss. One is due to spin-relaxation collisions, driven by the dipolar interaction between the electron spins of the two atoms. This component exists even in the absence of rf dressing, but is generally fairly small, both because the dipolar interaction is weak and because there is a centrifugal barrier in the outgoing channel. It is modified near the trap center because the rf-dressed states are mixtures of different spin states, and drops to zero on the low-field side of the trap, where the adiabatically trapped state correlates with lowest state in the magnetic field. The second component, which we refer to as rf-induced loss, is potentially stronger; the inelastic collisions are driven by the difference between the singlet and triplet interaction potentials, and there is no centrifugal barrier in the outgoing channel.

For ^{87}Rb in $f = 1$ states, the calculated rate coefficient for rf-induced loss is very small. We obtain $k_2^{\text{max}} = 1.25 \times 10^{-20} \text{ cm}^3 \text{ s}^{-1}$ at the trap center for an rf field strength

$B_{\text{rf}} = 0.5$ G. This is much smaller than the rf-modified spin-relaxation loss rate coefficient for ^{87}Rb .

We have explored the dependence of the rf-induced loss rate on the singlet and triplet scattering lengths a_s and a_t , and find that it can change by 10 orders of magnitude as the scattering lengths are varied. It is generally small when $a_s \approx a_t$, but may be enhanced by resonances of two different types. ^{87}Rb is a very special case: not only is a_s very similar to a_t , but their actual values are such that there is no enhancement by either type of resonance. Other alkali-metal atoms will generally have much larger rf-induced loss rates. For ^{39}K , which is a more typical case, we obtain $k_2^{\text{max}} = 6.33 \times 10^{-14} \text{ cm}^3 \text{ s}^{-1}$ for $B_{\text{rf}} = 0.5$ G. This is much larger than the rf-modified spin-relaxation loss rate, and 6 orders of magnitude larger than for ^{87}Rb . The rf-induced loss rate at the trap center increases at lower rf field strengths.

We have also investigated rf-induced loss for alkali-metal atoms in their upper hyperfine states, $f = 2$ for

^{87}Rb and ^{39}K . These losses are also small when $a_s \approx a_t$. In this case there are no Feshbach resonances, but the loss rates may still be enhanced by entrance-channel effects when $|a_t|$ is large. The rf-induced loss rates also depend strongly on the atomic hyperfine splitting, increasing as the hyperfine splitting decreases because of mixing of atomic f states by the magnetic field.

ACKNOWLEDGMENTS

We are grateful to Prof. C. J. Foot and Mr. E. Bentine for interesting us in this project and to them, Dr. M. D. Frye and Dr. C. R. Le Sueur for valuable discussions. This work has been supported by the UK Engineering and Physical Sciences Research Council (Grants No. ER/I012044/1, EP/N007085/1 and EP/P01058X/1 and a Doctoral Training Partnership with Durham University).

-
- [1] O. Zobay and B. M. Garraway, Phys. Rev. Lett. **86**, 1195 (2001).
 - [2] O. Zobay and B. M. Garraway, Phys. Rev. A **69**, 23605 (2004).
 - [3] B. M. Garraway and H. Perrin, J. Phys. B **49**, 172001 (2016).
 - [4] Y. Colombe, E. Knyazchyan, O. Morizot, B. Mercier, V. Lorent, and H. Perrin, Europhys. Lett. **67**, 593 (2004).
 - [5] W. H. Heathcote, E. Nugent, B. T. Sheard, and C. J. Foot, New J. Phys. **10**, 043012 (2008).
 - [6] T. Schumm, S. Hofferberth, L. M. Andersson, S. Wildermuth, S. Groth, I. Bar-Joseph, P. Krüger, and J. Schmiedmayer, Nature Physics **1**, 57 (2005).
 - [7] M. Göbel, *Low Dimensional Traps for Bose-Fermi Mixtures*, Ph.D. thesis, Ruperto-Carola University, Heidelberg (2008).
 - [8] N. Lundblad, P. J. Lee, I. B. Spielman, B. L. Brown, W. D. Phillips, and J. V. Porto, Phys. Rev. Lett. **100**, 150401 (2008).
 - [9] M. Shotton, D. Trypogeorgos, and C. Foot, Phys. Rev. A **78**, 051602(R) (2008).
 - [10] K. A. Burrows, H. Perrin, and B. M. Garraway, Phys. Rev. A **96**, 023429 (2017).
 - [11] T. V. Tscherbul, T. Calarco, I. Lesanovsky, R. V. Krems, A. Dalgarno, and J. Schmiedmayer, Phys. Rev. A **81**, 050701(R) (2010).
 - [12] T. M. Hanna, E. Tiesinga, and P. S. Julienne, New J. Phys. **12**, 083031 (2010).
 - [13] D. J. Owens, T. Xie, and J. M. Hutson, Phys. Rev. A **94**, 023619 (2016).
 - [14] E. Arimondo, M. Inguscio, and P. Violino, Rev. Mod. Phys. **49**, 31 (1977).
 - [15] Different papers use Hamiltonians corresponding to different definitions of B_{rf} . In particular, our previous work [13] used the same definition of B_{rf} as here for σ_X but a different normalization for σ_+ and σ_- . To match the present definition, the values of B_{rf} given in ref. [13] must be divided by $\sqrt{2}$ for σ_+ and σ_- polarization. Note that Hanna *et al.* [12] use spin raising and lowering operators normalized by $1/\sqrt{2}$ with respect to ours.
 - [16] C. Strauss, T. Takekoshi, F. Lang, K. Winkler, R. Grimm, J. Hecker Denschlag, and E. Tiemann, Phys. Rev. A **82**, 052514 (2010).
 - [17] S. Falke, H. Knöckel, J. Friebe, M. Riedmann, E. Tiemann, and C. Lisdat, Phys. Rev. A **78**, 012503 (2008).
 - [18] J. M. Hutson, E. Tiesinga, and P. S. Julienne, Phys. Rev. A **78**, 052703 (2008), note that the matrix element given in Eq. A2 of this paper omits a factor of $-\sqrt{30}$ and that for Eq. A5 omits a factor of $\frac{1}{2}$.
 - [19] J. M. Hutson and C. R. Le Sueur, "MOLSCAT: a program for non-reactive quantum scattering calculation of atomic and molecular collisions," (2017), manuscript in preparation.
 - [20] M. H. Alexander and D. E. Manolopoulos, J. Chem. Phys. **86**, 2044 (1987).
 - [21] J. M. Hutson, New J. Phys. **9**, 152 (2007).
 - [22] M. T. Cvitaš, P. Soldán, J. M. Hutson, P. Honvault, and J. M. Launay, J. Chem. Phys. **127**, 074302 (2007).
 - [23] M. Gröbner, P. Weinmann, E. Kirilov, H.-C. Nägerl, P. S. Julienne, C. R. Le Sueur, and J. M. Hutson, Phys. Rev. A **95**, 022715 (2017).
 - [24] G. F. Gribakin and V. V. Flambaum, Phys. Rev. A **48**, 546 (1993).
 - [25] C. J. Myatt, E. A. Burt, R. W. Ghrist, E. A. Cornell, and C. E. Wieman, Phys. Rev. Lett. **78**, 586 (1997).
 - [26] P. S. Julienne, F. H. Mies, E. Tiesinga, and C. J. Williams, Phys. Rev. Lett. **78**, 1880 (1997).
 - [27] F. H. Mies, C. J. Williams, P. S. Julienne, and M. Krauss, J. Res. Natl. Inst. Stand. Technol. **101**, 521 (1996).